Optimal Low-Power Piezoelectric Actuator Control With Charge Recovery for a Microrobotic Leg

Biju Edamana and Kenn R. Oldham, *Member, IEEE*

***Abstract*—This paper describes an efficient control strategy for a piezoelectric microactuator using charge recovery. For piezoelectric actuators, as well as other actuators that behave primarily as capacitive loads, energy consumption can be reduced by minimizing the number of times an actuator is charged and by recovering stored energy when it is turned OFF. An integer programming-based algorithm is used to drive microrobotic legs powered by piezoelectric actuators to a specified angle in a specified time using minimum energy. Partial charge recovery is incorporated; this allows the use of a more flexible controller than a pure ON–OFF controller, with two or more intermediate voltage levels between the minimum and maximum voltages available to improve positioning accuracy. Simulated and experimental tests show that a prototype piezoelectric robotic leg joint achieved controlled movements with one third of the energy consumed by a pure ON–OFF controller.**

***Index Terms*—Integer programming, microactuators, microelectromechanical devices, ON–OFF control, piezoelectric devices, switched systems.**

I. Introduction

RECENT developments in the area of microelectromechanical system (MEMS) actuators provide opportunities to develop extremely small autonomous devices such as mobile microrobots. In order to fulfil their potential, these devices should carry their own power source. This applies a strict constraint on the energy available to the device, as energy sources and associated power electronics circuitry must also be miniaturized. Hence, it is essential to make maximal use of scarce energy to prolong the duration of productive time. Although some miniaturized circuitry and power sources are already available, minimization of their energy consumption while meeting servo system constraints is sometimes difficult with conventional controller optimization methods. In this paper, an integer programming based optimization algorithm for such a system is discussed, specifically the prescribed rotation of the microrobotic leg joints with minimum power and an integrated charge recovery system. The effects of system design on inductor size and thus total mass savings given a specified power source is also discussed with regard to potential millimeter- or centimeter-scale microrobots.

Manuscript received November 11, 2011; revised March 11, 2011 and June 27, 2011; accepted July 19, 2011. Date of publication October 6, 2011; date of current version September 12, 2012. Recommended by Technical Editor S. Fatikow. This work was supported in part by the National Science Foundation, Grant CMMI #0965522, and in part by the Army Research Office, Grant W911QX-07-C-0072.

The authors are with the Department of Mechanical Engineering, University of Michigan, Ann Arbor, MI 48109 USA (e-mail: bij@umich.edu; oldham@umich.edu).

Color versions of one or more of the figures in this paper are available online at http://ieeexplore.ieee.org.

Digital Object Identifier 10.1109/TMECH.2011.2165079

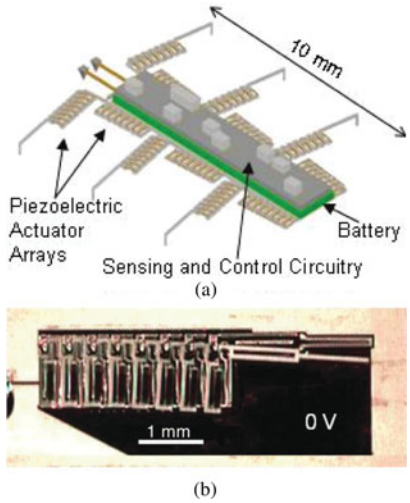

Fig. 1. (a) Concept-drawing of an autonomous microrobot based on thin-film piezoelectric actuator joint arrays. (b) Sample image of prototype leg joint at 0V, courtesy U.S. Army Research Laboratory.

Although a variety actuation schemes are available in the MEMS field, many have disadvantages for autonomous mobile microrobotics. High power consumption in thermal actuators requires a heavy power source [1]–[3], despite large force capacities. Although power consumption is low in electrostatic actuation, force produced per unit area by conventional comb-drive and parallel plate actuators is typically small [4]. Scratch drives with electrostatic actuation have larger force capacity but can perform only on a certain substrates and are more appropriate for much smaller devices [5], [6]. In comparison, piezoelectric actuators have light weight, high bandwidth, high force production, and lower power consumption [7], [8]. They are versatile and can be designed for producing large force over a small stroke length or large stroke length with smaller force, though they require substantially more complex fabrication processes to manufacture. By combining a number of actuators in series, a large force over a large stroke length can be achieved. Previous thin-film piezoelectric actuators utilizing novel release strategies to integrate piezoelectric and semiconductor materials have generated up to 3×10^{-9} N·m of work from a 500 μm $\times$ 100 μm area [9]. The same individual actuator designs used in this project can produce up to 3 degrees or more rotational motion at 20 V when coupled to microrotating leg joints with large weight bearing capacity. They may also be combined in series to produce substantial rotation required for a micro robotic leg joint, as in Fig. 1(b). Some less common electrostatic actuator designs [10] do produce amounts of work comparable to piezoelectric devices; the control strategy proposed here,

targeted for capacitive loads, is applicable to such actuators as well.

A major challenge in using piezoelectric actuators for autonomous microsystems is the associated power electronics when regulating the distance of actuator travel. Traditional analog amplifiers are designed to operate on resistive loads. However, piezoelectric actuators act primarily as capacitors. In a pure capacitive load, the phase angle between the voltage and current is 90 degrees, compared to zero degrees in a pure resistive load. Main et al. in [11] showed that when applied to piezoelectric actuators, traditional analog amplifier based circuits consume as much as or more than 95% of the energy supplied. They proposed an alternate option, using pulse-width-modulation (PWM) based switching controller circuits to compensate for these losses. This strategy reduces the energy lost in the circuit drastically, though in a switching controller the energy used by a capacitive load remains proportional to the frequency of switching. By minimizing the number of input voltage transitions using ON–OFF control, further energy can be saved, as in previous work [12] that minimized the number of switchings for a given motion of the actuator. In other words, once power electronics considerations limit inputs to the actuators to a finite number of switched voltages, controller timing of switching transitions becomes necessary to produce variable step distances.

These energy savings are made on the charging side of the actuator, but energy can also be saved upon discharge. When voltage is applied across a piezoelectric actuator (depending on its electromechanical coupling coefficient), a fraction of energy does the mechanical work and the remainder is stored as mechanical and electrical energy. When the applied voltage is removed, the actuator returns to the original position and the stored energy is drained off [11] and [13] showed that most of this energy can be recovered by a charge recovery circuit using an inductor connected to a storage capacitor.

In applying charge recovery schemes to small microactuators, resistances in the electrical interconnects and/or a need to limit inductor size (and thus mass) may prevent full charge recovery. If resistance is very small, theoretically it is possible to recover nearly all the entire energy drained from the actuator using a large, and hence heavy, inductor which is unsuitable for this application. Thus, the relationship between interconnect resistance, inductor size, and corresponding savings in overall weight of the power system must be considered. As a benefit, however, incomplete recovery leaves voltage levels on the actuator between the pure 'ON' and 'OFF' voltages. We refer to these additional voltage levels as intermediate voltage levels.

Intermediate voltage levels allow switching control using charge recovery to be more flexible and achieve tighter tolerance levels with regards positioning error when switching can be performed at finite sampling times. This corresponds to the precision with which a given leg joint moves to a desired position at a desired time, under nominal operating conditions. This is anticipated to help coordinate multiple leg joints in microrobotic prototypes with relatively low microcontroller sampling rates. Controller optimization includes scenarios, such as those in this paper, where a strict energy budget and high power consumption of sensor circuitry restrict the use of feedback, although the algorithm discussed can be extended using a receding optimization horizon to incorporate feedback. Previous usages of charge-recovery ([11] and [13]) did not take into account optimal controller design with few switched transitions, nor the opportunity to utilize intermediate voltage levels; previous work by the authors ([12]) has only considered the ON–OFF case.

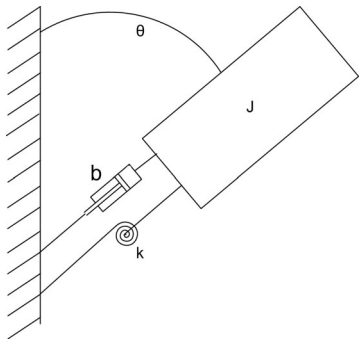

Fig. 2. Dynamic model of the leg joint.

The paper is organized as follows. Section II presents the system model. In Section III, the electrical circuit model of the system is presented. Section IV discusses the structure of the optimization problem and solving method used. Section V describes the experimental set up, results obtained from the application of pure ON–OFF and one of the charge recovery strategies, a simulation study on other charge recovery strategies, experimental evaluation of degradation in performance due to incorrect system identification and a simulational study conducted to investigate the possibility of a second actuator as a storage capacitor. Section VI discusses sizing of components given features of the microactuator to be controlled and power sources available. The last section discusses the contributions of the paper.

II. Dynamics of the System

A sample image of a microrobot leg joint is given in Fig. 1(b). The dynamics of this leg can be lumped into a mass-spring-damper system as shown in Fig. 2. An approximation of dynamics can be represented by a second order differential equation of the form

$$J\ddot{\theta} + b\dot{\theta} + k\theta = Gu \tag{1}$$

where J, b, and k denote the inertia, damping and stiffness of the joint, respectively, G represents the actuator gain, and u is the input voltage to the actuator. This can be converted to state space with states of the angle of rotation (θ) and the angular velocity ($\dot{\theta}$) of the actuator

$$\begin{aligned} \dot{x} &= A_c x + B_c u \\ y &= C_c x \end{aligned} \tag{2}$$

where

$$x = \begin{bmatrix} \theta \\ \dot{\theta} \end{bmatrix}$$

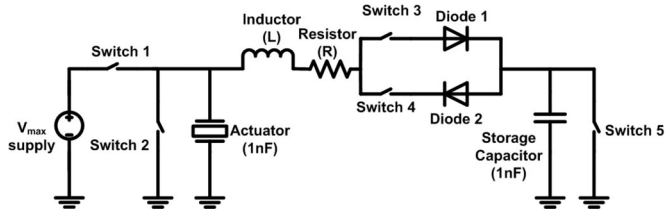

Fig. 3. Charge recovery circuit.

$$A_c = \begin{bmatrix} 0 & 1 \\ -k/J & -b/J \end{bmatrix}, B_c = \begin{bmatrix} 0 \\ G/J \end{bmatrix}$$

and

$$C_c = \begin{bmatrix} 1 & 0 \end{bmatrix}.$$

In general, these continuous equations can be replaced by a set of linear equations by discretizing them at sampling times T_s

$$x\left((k+1)T_s\right) = A_d x(kT_s) + B_d u(k)$$
$$y(kT_s) = C_d x(kT_s). \tag{3}$$

We note that while this paper deals specifically with the second-order robot leg model, the control strategies presented are valid for any actuator that is a capacitive load with discretized, linear dynamics. We assume that the initial conditions of the system are known. Hysteresis is not included in the robot leg model because its effects have been measured to be minor in the experimental robot leg tested (equivalent to less than a 10% variation in stiffness or gain parameters, at worst, as documented in [12]). This is a combined effect of comparatively small hysteresis of thin-film piezoelectric layers after poling at an elevated voltage and of the flexural stiffness of the leg due to the stiffness of silicon structures, which operate in a very linear elastic range. If hysteresis were to be more significant in a piezoelectric actuators operation, its effects could be incorporated into automatons describing charge recovery circuit operation, as will be described later.

Two important constraints on the system input exist. The first is that the inputs can be changed only at the sampling instants, determined either by the designer or the limitations of the microcontroller operating the system. The second constraint is on the values that input voltage $u(k)$ can take at each sampling instant when a charge recovery system is coupled with a switching, ON–OFF input. These constraints are explained in the following section.

III. Electrical Model of the System

A sample charge recovery circuit used for this study, nearly identical to that utilized by [13], is given in Fig. 3. The main difference in this circuit is the size of the inductor. Here, a smaller (and thus lighter) inductor is used than would provide nearly full charge recovery (discharge nearly to 0 V, or $V_{\min}$, and recharge nearly to the initial voltage on the actuator); in addition, resistances in the system may be much larger for the piezoelectric devices studied here, which also limits the degree of charge recovery. Optimal efficiency of the charge recovery circuit alone is achieved if the storage capacitor has the same capacitance as the actuator; approximately matched capacitors are used in this paper (with certain cases treating the storage capacitor as being a second actuator). A supply of voltage $V_{\max}$ is assumed to be connected to the actuator through switch 1. In practice, this voltage must be generated from some power source, typically batteries with operating voltage smaller than $V_{\max}$, either in series or connected to a voltage boost converter. Regardless of configuration, the ability to reduce direct charging events to the maximum voltage via a charge recovery circuit helps to reduce the amount of energy that must be provided at $V_{\max}$. This can be quite important, as the efficiency achieving $V_{\max}$ is often very poor for low-power devices.

Once the actuator is charged to $V_{\max}$, it can discharge itself through switch 2, or it can charge the storage capacitor when switch 3 closes. Then, the stored energy can be returned to the actuator through switch 4 or discharged to ground through switch 5. Only one of switch 1 to 4 can be turned on at a time and switch 5 may be turned on only when switch 3 and switch 4 are in the OFF position.

Further explanation is required for the modes when either switch 3 or 4 are closed. Consider the situation when the actuator voltage is greater than the storage capacitor voltage. In order to transfer charge from the actuator to storage capacitor, switch 3 is closed. During the time that the current flows from actuator to storage capacitor the circuit can be modeled as a second order system in terms of charges stored in actuator q_1 and storage capacitor q_2 (4). For effective charge recovery, circuit parameters are chosen to produce an underdamped system that will give an overshoot in the circuit response and result in more energy savings than connecting the capacitors directly without any inductor. The diode present in the circuit will prevent reverse current and will keep the capacitor voltages constant at the overshoot points. Charge dynamics, assuming equal actuator and storage capacitance, become

$$L(\ddot{q_1} - \ddot{q_2}) + R(\dot{q_1} - \dot{q_2}) + \frac{q_1 - q_2}{C/2} = V_D \tag{4}$$

where V_D is the voltage drop across the diode. Letting $q_1(0) = V_{10}C$, $q_2(0) = V_{20}C$, and the differential voltage $V = (q_1 - q_2)/C$, where V_{10} and V_{20} are the initial voltages on actuator and storage capacitor, respectively.

$$L\ddot{V} + R\dot{V} + \frac{V}{C/2} = \frac{V_D}{C}$$
$$V(0) = V_{10} - V_{20}. \tag{5}$$

Assuming that $V_{10} > V_{20}$ before switching, then $V(t)$ will follow a step response until it reaches the maximum value and will remain there because of the diode. A typical response is shown in Fig. 4. The response of the system up to the overshoot point then can be written as

$$V(t) = V_D + (V(0) - V_D)e^{-\alpha t}\left(\cos\beta t + \frac{\alpha}{\beta}\sin\beta t\right) \tag{6}$$

where $\alpha = \frac{R}{2L}$ and $\beta = \frac{\sqrt{\frac{8L}{C} - R^2}}{2L}$.

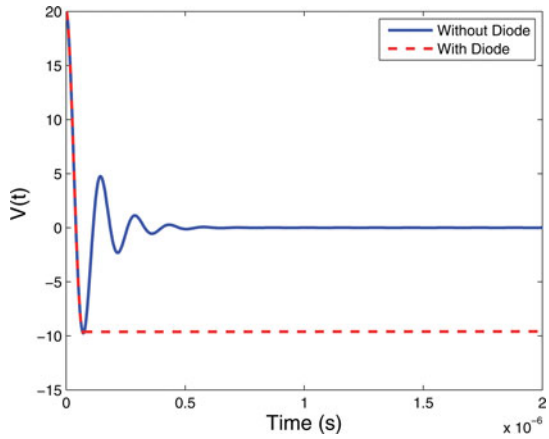

Fig. 4. Typical variation in the differential voltage for circuit parameters $L = 1\,\mu H, R = 20\,\Omega, C = 1\,nF$ and ideal voltage drop in the diode.

$V(t)$ reaches its maximum value when $t = \frac{\pi}{\beta}$ and the corresponding differential voltage will be the difference between the actuator voltage, V_{11}, and the storage capacitor voltage, V_{21}, after switching.

$$V_{\max} = V_{11} - V_{21} = V_D - (V(0) - V_D)e^{-\frac{\alpha\pi}{\beta}}. \quad (7)$$

The above equation together with the charge conservation equation

$$C(V_{10} + V_{20}) = C(V_{11} + V_{21}) \quad (8)$$

can be used to evaluate the actuator voltage and the storage capacitor voltage after switching

$$V_{11} = V_D\left(\frac{1+\mu}{2}\right) + V_{10}\left(\frac{1-\mu}{2}\right) + V_{20}\left(\frac{1+\mu}{2}\right) \quad (9)$$

$$V_{21} = -V_D\left(\frac{1+\mu}{2}\right) + V_{10}\left(\frac{1+\mu}{2}\right) + V_{20}\left(\frac{1-\mu}{2}\right) \quad (10)$$

where $\mu = e^{-\frac{\alpha\pi}{\beta}}$. Using a diode with negligible voltage drop compared to the maximum actuator voltage, the above equations can be approximated to form symmetrical equations

$$V_{11} = V_{10}\left(\frac{1-\mu}{2}\right) + V_{20}\left(\frac{1+\mu}{2}\right) \quad (11)$$

$$V_{21} = V_{10}\left(\frac{1+\mu}{2}\right) + V_{20}\left(\frac{1-\mu}{2}\right). \quad (12)$$

These equations are derived for the case when the actuator voltage is greater than the storage capacitor voltage. If the storage capacitor voltage is higher, the charge can be returned to the actuator by closing switch 4 (and opening switch 3); the equations are still valid.

It should be noted that the electrical model above can be equally applied to other capacitive actuators, such as electrostatic MEMS actuators. The optimization that follows may be used on such systems as well, in combination with a linearized version of mechanical system dynamics in the form of (1). One difference is that parasitic capacitances would be more prominent in an electrostatic actuator or for other piezoelectric materials. The high dielectric constant of lead-zirconate-titanate, used here, causes actuator capacitance to be larger than parasitic capacitances in the system, which would not necessarily be true for other microscale capacitive actuators.

IV. Optimization Method

A. Objective Function

The objective of the optimization is to drive the states of the system θ and $\dot{\theta}$ given in (1) to a desired set of values in a prescribed time using minimum energy. Hence, the objective function is the energy used by the actuator directly from the power source. This energy consumption can be divided into two parts. The first part is termed as capacitive loss J_C, consumed whenever the actuator is charged using external power or, in other words, when a transition in voltage states on the actuator occurs that is powered externally. In general, this can be written as

$$J_C = \sum_{k=1}^{n} C(u_{\text{switch}_1}(k)(u(k)^2 - u(k-1)^2) + u_{\text{switch}_1}(0)u(0)^2) \quad (13)$$

where C is the capacitance of the piezoelectric actuator and $u_{\text{switch}_1}(k)$ is a binary variable which takes value 1 if switch 1 is on at k^{th} time instant and 0 otherwise and $u(k)$ represents the voltage on the actuator at the k^{th} instant, which can take any allowed voltage given in the automata described in the following section. The $u(0)$ term influences the cost if the controller calls for direct charging from the power supply at the initial time step from a standby voltage of 0 for individual motions or the final voltage at the last time step for repeated motions.

The second portion of possible energy use is a resistive loss denoted by J_R which occurs during the time when the actuator is externally powered

$$J_R = \sum_{k=0}^{n} \frac{u(k)^2}{R_l} T_s u_{\text{switch}_1}(k) \quad (14)$$

where R_l is the resistance of the system to leakage current and T_s the sampling time used for discretization. In piezoelectric films with high leakage resistance, resistive loss is negligible over short movement duration compared to capacitive loss, and hence it is not considered in the optimization.

B. Constraints

Three types of constraints exist in the optimization problem: the dynamics of the system, the final desired states, and the constraints on the inputs, explained in the following sections.

1) System Dynamics Constraints: The system dynamics form pn equality constraints from (3) during optimization, as given below. Without loss of generality, it is assumed that the system starts from the zero initial state. Here p is the order of the system, being $p = 2$ for the second-order system in this paper, and n is the number of time steps allowed to reach the final desired states as explained in the next paragraph

$$x((k+1)T_s) = A_d x(kT_s) + B_d u(k). \quad (15)$$

2) Final State Constraints: Since the inputs can be changed only at certain instants and can take only certain values, it is impossible to drive the states to arbitrary points in the state space. Instead, the aim is to reach the neighborhood of a desired final state as shown by $x(n * T_s) \in [x_d \pm \epsilon]$. This forms p inequality constraints. The bound ϵ can be selected based on the level of precision desired for a given motion. In the case of a microrobot, this would correspond to the error permitted in each leg's motion under nominal conditions at the end of a single stepping motion by multiple legs. In this paper, an arbitrary tolerance of 0.001 rad on joint rotation is used, and the method may be applied in the same manner for other tolerances depending on robot need. It is possible that if large errors may be tolerated, errors in robot motion may not be improved by the intermediate voltage levels provided by charge recovery compared to pure ON–OFF control (though power savings may be possible). Even then, we anticipate that a controller using intermediate charge recovery could maintain a given tolerance at lower sampling rates than a pure ON–OFF controller, with benefits for power consumption for computation.

3) Input Transition Constraints: This set of constraints is the difference between the current problem and previous, optimal ON–OFF control problems [12]. In a simple ON–OFF controller the input u_k can take either voltage levels of $V_{\min}$ or $V_{\max}$ only with transitions happening at the sampling instant. In the partial charge recovery problem discussed here, the input voltages can take certain intermediate voltage levels in between $V_{\min}$ and $V_{\max}$, depending on the size of the components (primarily the inductor and resistance) in the charge recovery circuit as given in (7). The voltages between $V_{\min}$ and $V_{\max}$ are referred to as intermediate voltages below. Different scenarios for use of the charge recovery circuit are described below.

Strategy 1 (Static charge recovery): A simple strategy was considered first. The storage capacitor discharges any remnant energy after the actuator is charged or before the actuator is discharged to it, effectively resetting the states of the automaton after each cycle of discharging to and charging from the storage capacitor. By this assumption, the intermediate voltages can be predetermined.

In this scenario, the actuator is charged to $V_{\max}$ when switch 1 turns on and it will either drain the charge to ground through switch 2 or it will charge the storage capacitor through switch 3. If it drains the energy the actuator voltage will go back to $V_{\min}$ and if it charges the storage capacitor the actuator voltage will reach $V_{\text{Intermediate}_1}$. From $V_{\text{Intermediate}_1}$ the actuator can return to $V_{\min}$ or $V_{\max}$, but the storage capacitor will drain all its energy. If the actuator recovers the charge through switch 4, it will attain $V_{\text{Intermediate}_2}$. From this state, actuator voltage may be maintained, fully charged or discharged. This results in just four voltage levels as shown in the automaton given in Fig. 5. The states of the automaton represent the actuator voltage at each instant of time.

In order to convert these constraints to equations, a new set of binary variables v_1, v_2, v_3, v_4 are introduced, each corresponds to an input voltage in the set $V_{\min}, V_{\max}$, $V_{\text{Intermediate}_1}, V_{\text{Intermediate}_2}$. Input voltage at time $t = k * T_s$

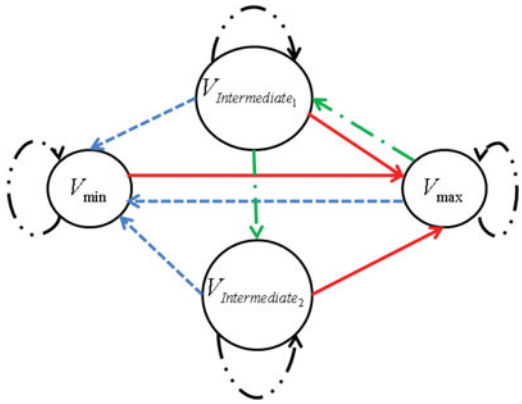

Fig. 5. Automaton showing the constraints on actuator voltage transitions for the simplest case.

can be written as

$$u(k) = v_1(k)V_{\min} + v_2(k)V_{\max} + v_3(k)V_{\text{Intermediate}_1} + v_4(k)V_{\text{Intermediate}_2} \quad (16)$$

and the following constraint ensures that the system is in only one state at a time (note that $v's$ are binary):

$$v_1(k) + v_2(k) + v_3(k) + v_4(k) = 1 \ \forall k \in 0 \ldots n. \quad (17)$$

Additional constraints ensure illegal transitions, such as a transition from $V_{\max}$ to $V_{\text{intermediate}_1}$, do not happen. This can be done by making sure that $v_2(k)$ and $v_3(k+1)$ are not simultaneously one, as by the inequality constraint $v_2(k) + v_3(k+1) \leq 1$.

Strategy 2 (Dynamic charge recovery): In the second strategy, we remove constraints on the transitions of storage capacitor voltages. This is more challenging to optimize, but it has greater potential to improve the efficiency of the system. The intermediate actuator and storage capacitor voltages are not constants in this case. The values the voltages can take at any point of time $t = (k+1)T_s$ depends on the charge stored in the actuator and storage capacitor at the previous instant kT_s. At time $t = kT_s$ let the voltages on actuator and storage capacitor be V_{10} and V_{20}, respectively. Then at next instant the actuator voltage can take any of the following values $\{V_{\min}, V_{\max}, V_{10}[\frac{1-\mu}{2}] + V_{20}[\frac{1+\mu}{2}]\}$ and the storage capacitor voltage can take any value from the set $\{V_{\min}, V_{20}[\frac{1-\mu}{2}] + V_{10}[\frac{1+\mu}{2}]\}$. The derivation of these voltages was shown in (7).

This problem has a new nonlinear constraint to make sure that the actuator voltage and the storage capacitor voltage are one of those allowed at the current time instant, as described later. The binary variables $w_1(k) \ldots w_7(k)$ ensure that the state in the automaton, represented in the form (actuator voltage, storage capacitor voltage), is one of the allowed automaton states, as shown in Fig. 6, which represents a system of allowed binary switching sequences

$$u(k) = w_1(k)V_{\max} + w_2(k)V_{\min} + w_3(k)\left(u(k-1)\left[\frac{1-\mu}{2}\right] + u_s(k-1)\left[\frac{1+\mu}{2}\right]\right)$$

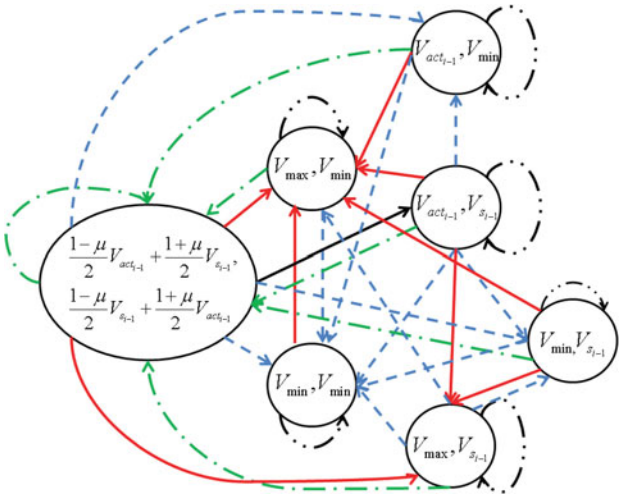

Fig. 6. Automaton showing the constraints on the input voltage for the case 2.

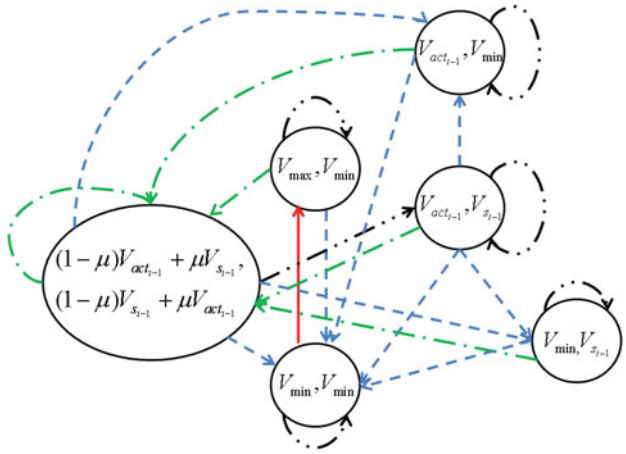

Fig. 7. Automaton showing the constraints in the modified optimization.

$$+ w_4(k)u(k-1) + w_5(k)u(k-1) + w_6(k)V_{\max} + w_7 V_{\min} \quad (18)$$

$$u_s(k) = w_1(k)V_{\min} + w_2(k)V_{\min} + w_3(k)\left(u_s(k-1)\left[\frac{1-\mu}{2}\right] + u(k-1)\left[\frac{1+\mu}{2}\right]\right) + w_4(k)V_{\min} + w_5(k)u_s(k-1) + w_6(k)u_s(k-1) + w_7 u_s(k-1) \quad (19)$$

$$w_1(k) + w_2(k) + w_3(k) + w_4(k) + w_5(k) + w_6(k) + w_7(k) = 1. \quad (20)$$

Here, $u(k)$ and $u_s(k)$ are actuator voltage and storage capacitor voltage at time $t = kT_S$, respectively. Some of these constraints are nonlinear due to the multiplication of real variables with binary variables. This type of constraints can be converted to a set of linear constraints by introducing a set of new variables by the following procedure [14]. Consider a new variable $z(k)$, to replace the term $w_4(k)u(k-1)$ in (18). By adding the following four additional linear constraints, the above equation can be converted to a linear equation on z:

$$\begin{aligned} z(k) &\le M w_4(k) \\ z(k) &\ge m w_4(k) \\ z(k) &\le u(k-1) - m(1 - w_4(k)) \\ z(k) &\ge u(k-1) - M(1 - w_4(k)) \end{aligned} \quad (21)$$

where $M = \max(u(k-1)) = V_{\max}$ and $m = \min(u(k-1)) = V_{\min}$. Similarly, each of the product terms are replaced by new variables and additional linear constraints are added.

The constraints on transitions of actuator voltage and storage capacitor voltage are shown in Fig. 6. The transitions marked by solid lines involve external power usage, dash-dot lines employ the charge recovery circuit, dash-dot-dot lines represent staying at the same state and dashed lines are discharge of either actuator or storage capacitor. From the initial optimization it was observed that the full range of possible leg motions (i.e., target final angles) can be achieved with one external powered charging of the actuator at the beginning of the motion. Thus, the problem of motion optimization may be extended to maximizing the energy stored in the storage capacitor at the end of the optimization horizon for future use.

Strategy 3 (Modified dynamic charge recovery): In cases where the energy consumption for a given rotation is the minimum possible (a single charging from the external power source for the range of possible actuator final angles) the optimization objectives were modified to better suit repeated motions. The new objective function is set to maximize the storage capacitor voltage at the end of the optimization horizon. By maximizing the final storage voltage more than one step of actuation can be achieved by one externally powered voltage switching for smaller leg motions, or the additional energy required to repeat the current motion can be minimized for larger leg motions.

$$J_{\text{modified}} = u_s(n) \quad (22)$$

where n is the number of allowed time steps to reach the desired final state as given the earlier section. An additional constraint was added to limit the number of times that the actuator was charged directly from the power supply to one for a given motion. Mathematically, this is done by limiting the number of transitions from ($V_{\min}$,$V_{\min}$) to ($V_{\max}$,$V_{\min}$) to one in the automaton given in Fig. 6 resulting in the automaton given in Fig. 7.

$$\sum_{k=0}^{n} w_2(k)w_1(k+1) \le 1. \quad (23)$$

This nonlinear constraint was converted to a linear one using the method shown in (21).

4) Hysteresis Approximation: While hysteresis effects are very small in the current application, the automaton description of the charge recovery system may also be expanded to approximate certain hysteresis effects in other piezoelectric actuators. To do this, states in the automaton reached from both larger and smaller voltages would be split into two separate states.

The state reached from a higher voltages could then report a larger effective voltage as entering the system, while the state reached from a lower voltage would report a smaller effective voltage, to simulate different gains of the piezoelectric actuator when voltage is decreasing or increasing. While not a perfect representation of true hysteresis behavior, this would produce an approximation of hysteretic effects, thanks to the fact that voltages on the actuator are reached from specific prior voltages based on the charge recovery sequence, particularly when using static charge recovery (strategy 1).

C. Optimization Solver

All three problems discussed above had linear constraints after the conversion given in (21). The first two strategies have quadratic objective functions and the third strategy includes a linear function. Due to the presence of binary variables the problem is NP-hard, so the optimization needs special integer programming techniques to be solved efficiently. A branch and bound method was used. In a branch and bound algorithm complete enumeration of the entire binary tree is done in a systematic manner. The entire solution space is explored and divided into feasible subdomains, then valid upper and lower bounds are derived for each subdomains. The infeasible and nonoptimal regions are eliminated (pruned) during the process, done using the fewest numerical operations possible. The combination of softwares AMPL and CPLEX was used generating solutions using the branch and bound method. AMPL was used to model the optimization problem and CPLEX for solving it.

V. Experimental and Simulational Results

A. Experimental Setup

Experiments were performed on two piezoelectric actuators, a macroscale cantilever actuator with natural frequency of approximately 30 Hz, and a microscale piezoelectric actuator with natural frequency of approximately 300 Hz fabricated by the U.S. Army Research Laboratory. System dynamics were identified from the step responses of the systems over relatively long time scales (0.15 and 0.015 s, respectively) and then controller performance was tested over a time duration of approximately half a period for each system (0.02 and 0.002 s, respectively). Conceptually, this choice of final time allows the use of the overshoot of the natural system dynamics to achieve a wider range of motion, but then applies careful timing of switching transitions to reach specified step lengths over this constant step time. Multiple legs might ultimately be coordinated during a given stepping period, followed by motion by another set of multiple legs.

Initial experiments were conducted on a macroscale piezoelectric actuator, which was also used to test dynamic charge recovery. The actuator is a 40-mm long, 10-mm wide Ceratec, Inc. bimorph actuator with an Omega, Inc. 1000 Ω precision parallel strain gauge attached by cold cure adhesive for measuring its deflection. The variations in strain gauge voltage were measured through a wheatstone half bridge circuit with a 1 kHz bandwidth low-pass filter added to reduce noise. The switching

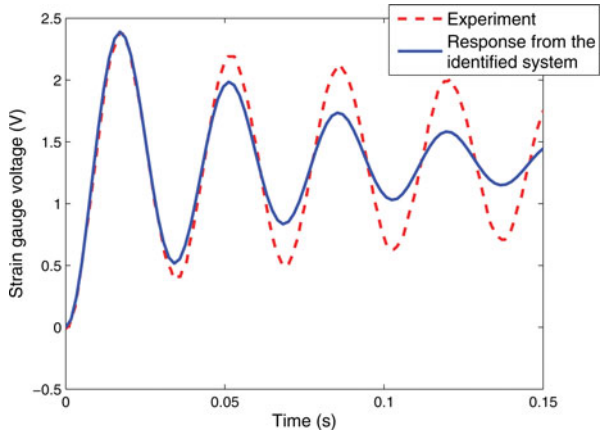

Fig. 8. Step response of the macro system for a 20 V input.

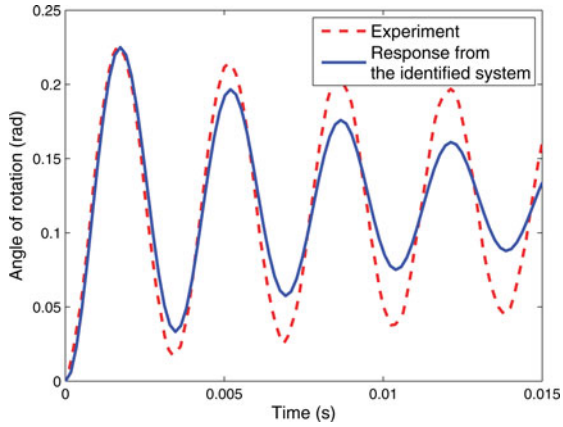

Fig. 9. Step response of the micro system for a 20 V input.

sequences were loaded into a TMS320F28335 microprocessor which was interfaced to the bimorph actuator through analog devices fast switches ADG5412BRUZ. First, a 20 V step input was applied to the system, and from the response obtained (Fig. 8) the following second order system was fitted between the input voltage and the strain gauge output voltage. In the charge recovery circuit, a $3mH$ inductor and a $3.6nF$ storage capacitor were used.

$$\frac{y(s)}{u(s)} = \frac{1}{4.4084 \times 10^{-4} s^2 + 0.0126s + 14.9254}. \tag{24}$$

The MEMS actuator, the prototype robotic leg shown in Fig. 1(b), was also operated using the microprocessor and the analog device switches. Motion of the rotational joint was captured using a high speed camera at 8000 frames per second and the angle of rotation was measured using the MATLAB Image Processing Toolbox. A step input of 20 V was applied on this actuator and the corresponding response is shown in Fig. 9. Displacement angles are averaged from many different locations along the rigid portion of the leg to reduce measurement error. The following second order system was identified between the input voltage and the angle of rotation of the leg in radians. In this case, the charge recovery intermediate voltages were 9.6 V

and 12.4 V for a 3.1 nF storage capacitor and 1 mH inductor.

$$\frac{y(s)}{u(s)} = \frac{1}{5.0039 \times 10^{-5} s^2 + 0.0093 s + 164.6091}. \quad (25)$$

From earlier studies, it was seen that the effect of hysteresis on actuator design discussed here is $\pm 10\%$ and the controller can be modified to improve robustness and to counter hysteresis [12]. Since satisfactory performance was obtained without adding the robustness method, hysteresis effects are not considered in the system identification. It is also evident from Fig. 9 that the purely linear system model is less accurate beyond the first oscillation of the underdamped free response, possibly due to nonlinear damping or higher-order mode effects. Again, however, the linear model is found to be sufficiently accurate to obtain satisfactory performance from the controlled response, largely because the studies to follow focus on the transient motion of the actuator over a time period comparable to the peak time in order to emulate a single step of a microrobot.

B. Comparison Between Simulation and Experimental Result on Microactuator

Results obtained from applying the static charge recovery (strategy 1) on the microactuator are discussed in this section. The identified second order system (25) was discretized using a sampling time of 0.1 ms. Final state constraints were to reach (0.130 ± 0.001 radians, ± 1 rad/s) at 2 ms. Higher tolerances on velocity, for both macro- and microscale systems, are chosen to give a similar relative error in the two states, as the high natural frequencies of the systems result in larger numerical ranges for velocity than displacement. The target final values were selected as an arbitrary step angle below the maximum displacement of the leg joint, as though instructing the leg to move a desired distance and reach zero velocity at a given time when it would be raised from or lowered to the ground in exchange with other legs on a robot. In this first study, the simplest charge recovery scheme was again used to find the optimal switching sequence. In the simulation the angle reaches 0.1297 radians at 2 ms, which is in the satisfactory range, and the experiment also follows very closely and settles around the same value as shown in Fig. 10(a). From the video-captured angular measurement it was verified that the actuator momentarily becomes stationary at the expected time with a displacement of 0.13 rad and less than the targeted 1 rad/s velocity. The actuator is externally charged only once.

C. Comparison With ON–OFF *Controller for Power Consumption*

The advantage of the charge recovery strategy over a simpler ON–OFF controller in terms of energy consumption was evaluated on the microscale system. An optimal ON–OFF switching sequence was calculated for a final state constraint of ($0.13rad \pm 0.001$ radians, ± 1 rad/s) at a final time of 2 ms, identical to the charge recovery case. Both the simulation and experimental responses, when these sequences are applied, are shown in Fig. 10(a) and (b). The simulation and experimental results match, and the ON–OFF controller switches three times to achieve the desired performance, as shown in Fig. 10(c). Hence,

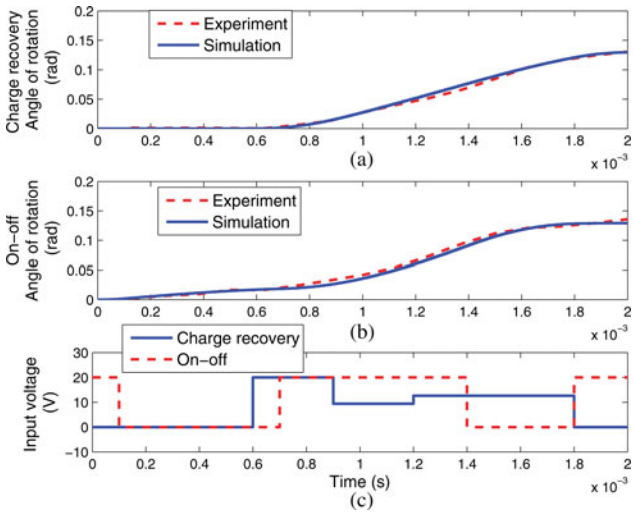

Fig. 10. (a) Micro system–Charge recovery controller response for an optimal sequence to reach 0.13 rad at 2 ms. (b) Micro system ON–OFF controller response for an optimal sequence for the same state constraints. (c) Optimal charge recovery controller and ON–OFF sequences.

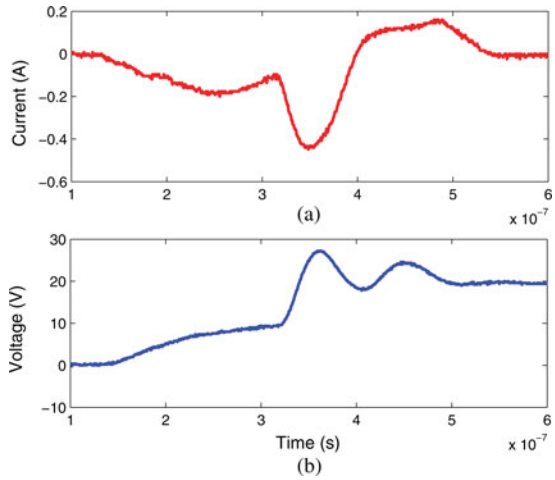

Fig. 11. Current consumption of switching circuitry and the MEMS actuator while the switch is turned on from 0 V to 20 V.

the ON–OFF controller consumes three times more power (approximately 0.6 μJ) than the charge recovery strategy consumed. It is also observed that the experimental motion with charge recovery is slightly more accurate than that using only ON–OFF control.

In order to verify the energy consumption in the experimental switching circuitry and the MEMS actuator, current and voltages were measured while the switch is turned on charging the actuator from 0 to 20 V. The switching happens in less than a microsecond, as shown in Fig. 11. The energy consumption was evaluated during this period from the current and voltage and found to be 0.27 μJ, as compared to an expected value of approximately 0.2 μJ for a nominal 1 nF capacitance; additional power consumption is attributed to a combination of underestimating the true capacitance and some parasitic capacitance occurring at the actuator. This results in an experimental energy

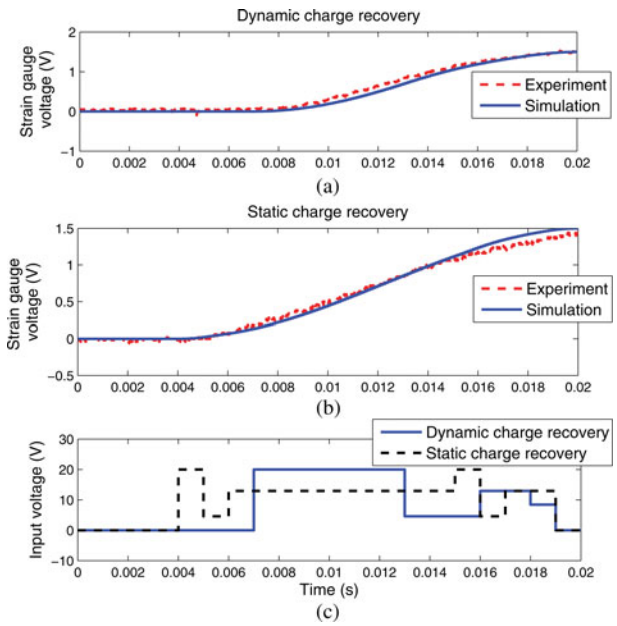

Fig. 12. (a) Macro system-dynamic charge recovery controller response for an optimal sequence to reach 1.5 V at 20ms. (b) Macro system static charge recovery controller response for an optimal sequence for the same state constraints. (c) Optimal dynamic and static charge recovery controller sequences.

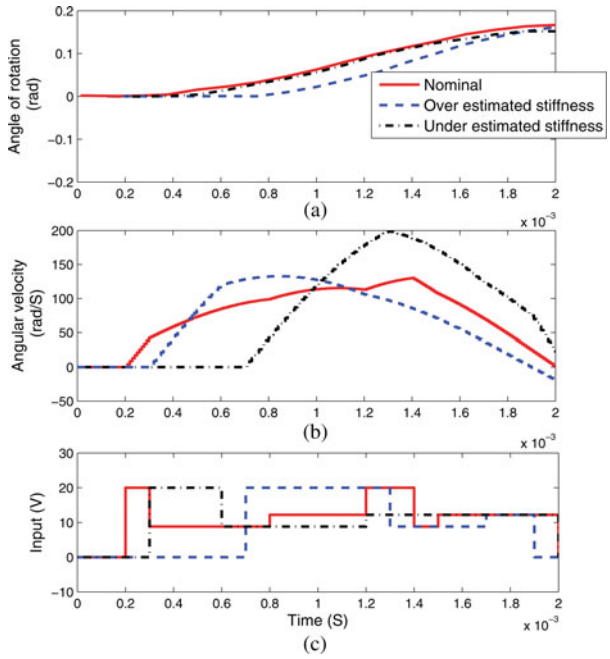

Fig. 13. Changes in response due to uncertainties in estimated system during the system identification.

consumption per step of 0.27 μJ for the charge recovery controller and 0.81 μJ for the ON–OFF controller.

In addition to experimental verification of movement to a variety of target angles, a wide variety of motions were compared in simulation. Depending on the error tolerance level specified, energy savings due to charge recovery varies, but is never worse than that of an ON–OFF controller and improvements as great as 80% were obtained for certain combinations of parameters. In addition, a larger number of combinations of angles, angular velocities and the tolerances are achievable with charge recovery using intermediate voltage levels than through ON–OFF control alone.

D. Experimental Evaluation of Multistage Charge Recovery With Dynamic Intermediate Voltages on Macroscale Actuator

Results obtained from experiments conducted on the macroscale actuator in comparing dynamic charge recovery (strategy 3) to static charge recovery (strategy 1) are discussed here. The identified second order system (24) was discretized using a sampling time of 1 ms. As an illustration, final state constraints are set to reach (1.5 $\pm$ 0.015 V, $\pm$10 V/s) at the strain gauge output at a final time of 20 ms. A charge recovery constant $\mu = 0.5410$ was found experimentally.

Experimental and simulation responses for the setup above are shown in Fig. 12(a) and (b). The corresponding optimal sequences are shown in Fig. 12(c). The static charge recovery sequence (dashed lines) switches between predetermined voltages (0 V, 4.6 V, 12.9 V, 20 V) and switches twice to 20 V. In contrast, the dynamic charge recovery strategy has more voltage options available and its input sequence (solid lines) switches only once to 20 V, hence consuming less energy. Moreover, the storage capacitor voltage at the end of this motion (11.6 V) can be used to help charge the actuator for the next set of motions.

Unfortunately, dynamic charge recovery was not successfully implemented on the microscale actuator, due to leakage current through the PZT thin-film. For the specific actuator tested, dynamic charge recovery simulations indicated advantage primarily for repeated motions, and during the time to return to its initial state, voltage levels on the actuator are found to change significantly; this return motion can require between 2 and 20 times as long as is required to make a given forward motion, depending the extent to which the return to the initial state is controlled. In addition, exact leakage current and capacitance values prove to be highly variable between wafers on which actuators are fabricated, indicating one limitation to control sequence optimization, especially for the more complex strategies.

E. Experimental Evaluation of Degradation in Performance Due to Incorrect System Identification

An experimental study was also conducted to evaluate the degradation in performance due to incorrect system identification. Since only a single actuator was available at this time, the identified model was artificially perturbed when calculating optimal input sequences. Initially, the system was identified using a step response and an optimal charge recovery switching sequence was calculated. In this case, the objective was to reach (0.15 ± 0.001 radians, $\pm$1 rad/s) at 2 ms. The nominal responses shown in Fig. 13 correspond to this input sequence. Then the stiffness was changed to 10% of its nominal value and new optimal sequences were calculated. The two responses in Fig. 13 correspond to the under and overestimated stiffness. The optimal sequences for each case are shown Fig. 13(c). The angular displacements were closely matched as shown in Fig. 13(a) and

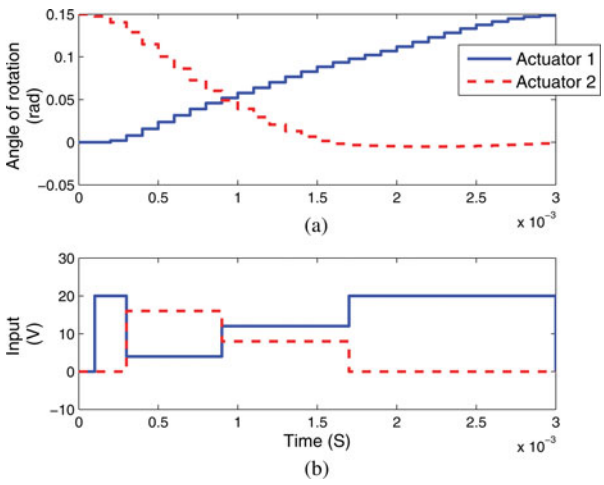

Fig. 14. Responses of two actuators while actuator 2 acts as a storage capacitor and returns to zero displacement state.

show little effect of incorrect system identification. On the other hand, the angular velocities at the final time for the under and overestimated stiffness do not satisfy the desired constraints, suggesting a need for careful identification if final values for both states are critical. Similar responses were obtained in experiments when the inertia terms were perturbed.

F. Simulation of a Second Actuator as a Storage Capacitor

A simulation study was also conducted to investigate the possibility of coordinating motion of two actuators in which one acts as a storage capacitor. This is intended to mimic the use of charge recovery in a robot utilizing two sets of legs, one set to drive the robot forward during a step and the other set returning to its nominal position over the same time period. The objective in this simulation was (0.15 ± 0.001 radians, 0 rad/s$\pm$1 rad/s) at 3 ms for actuator 1, which starts from a stationary position at 0 radians. Actuator 2, which acts as a storage capacitor starts from (0.15 rad, 0 rad/s), as though it has completed a step, and is desired to stop at 0 radians at 3ms. As can be seen in Fig. 14(a), the actuators achieved the desired goal. We observe from the study that this puts additional constraints on the optimization and the feasible region is smaller. Hence, an extended time period was found to be necessary to coordinate both legs effectively, and certain goals which were obtainable in the charge recovery of a single actuator alone may not be feasible when two actuators are combined.

VI. Discussion

Experimental testing and simulation results for the charge recovery control strategy described above indicate that substantial reductions in power consumption (66% or more in the test cases described) can be made when using charge recovery to operate a piezoelectric microactuator instead of pure ON–OFF control. This general approach is thus potentially useful as a power-saving measure for small actuators that behave as capacitive loads. However, for an untethered microrobot application, the key quantity to be reduced is the mass of the power source and power electronics in total, upon which inductor mass and assumptions about the power supply have a significant effect.

The intermediate voltage levels achieved by the charge recovery system depend on the damping ratio, ζ, of the resistor-inductor-capacitor circuit formed during switching. A smaller damping ratio results in closer to perfect charge recovery, and thus greater energy savings. In turn, the intermediate voltage levels dictate the number of times the actuator must be charged directly from the power supply, N_{charge}, compared to the number of times this would occur using an ON–OFF controller, $N_{\mathrm{on\text{-}off}}$, with these quantities determined by the controller optimization. The inductor size needed to achieve a given damping ratio can be estimated from the equation

$$L \approx \frac{R^2 C_{\mathrm{tot}}}{4\zeta^2} \tag{26}$$

which is based on the second order model for the circuit with C_{tot} equal to the total capacitance of actuators, C, storage capacitance, C_s, and parasitic capacitance, C_p being connected at one time. Resistance in the system, R, is a combination of resistance in the inductor, diode, and interconnects from the power electronics to the actuators themselves.

For the prototype microscale experimental system, with actuator capacitance of approximately 1.1 nF, parasitic capacitance of approximately 0.1-0.2 nF and a 2 nF storage capacitor, nearly complete charge recovery, say with a damping ratio less than 0.1, would require an inductor of about 15 mH, where a 1 mH inductor is sufficient to produce the partial charge recovery results discussed throughout the paper. However, this remains a very large inductor, which is primarily a consequence of very large resistance (400 Ω) in the electrical interconnects to the prototype actuator.

In contrast, direct connection of the charge recovery circuit to an equivalent discrete capacitor, such that resistance is primarily dictated by the resistance of the diode and inductor (approximately 10 Ω) indicates that comparable charge recovery can be obtained with inductors as small as 500 nH. The smallest inductor sizes are feasible for circuits with large inductor Q, low diode resistance, and a low diode reverse recovery time, with diode characteristics tending to be more influential in the experiments done to date. To reduce the interconnect resistance on chip to a comparable level, future actuators can use wider interconnects, more efficient interconnect routing, somewhat thicker electrode materials, and electroplate the entire interconnect with a thick gold film, which is currently applied only to portions of the actuators and interconnects.

A. Implications for Robotics

Even with a revised actuator design, 500 nH inductor is still reasonably large from the perspective of a millimeter- or centimeter-scale microrobot, with common inductors of that size (such as the 0402AF series) having a mass of approximately 1 mg. This is on the same order of magnitude as the projected payload of microrobots based on thin-film piezoelectric technology, previously calculated to range from about 0.5 to 200 mg [15], [16], with the dramatic range in payload dependent

on the number and configuration of legs and thickness of the silicon portions of the actuators (fewer, longer legs having low payload capacity and more, shorter legs having higher payload capacity, with relatively consistent piezoelectric capacitance in the various scenarios).

Whether the addition of charge recovery to a microrobot reduces the mass of the overall power system thus depends on system decisions, such as the stepping frequency of the robot gait, f, (which will decrease from the 500 Hz of the prototype leg joint as payload is added), power density of the battery used, ρ, and the efficiency, η, of any conversion method required to provide a voltage supply at $V_{\max}$, rather than a lower battery operating voltage. A large capacitor is taken to be present at the voltage converter or other power source output to deliver the peak power required during initial charging events, but such capacitor mass would typically be small compared to the inductor, and further modification might be required to manage efficiency of the battery discharge. As a rough approximation, though, battery mass saved, m_s, which must be greater than any additional electronics added to the system (primarily the inductor) in order to provide a systematic benefit, can be estimated from the equation

$$m_s \approx (C + C_p)\, V_{\max}^2 \frac{(N_{\text{on-off}} - N_{\text{charge}})}{\rho\eta} f. \qquad (27)$$

A representative scenario can thus be constructed using the intermediate voltages applied to the microscale actuator earlier in the paper (in other words, $N_{\text{on-off}} = 3$ reduced to $N_{\text{charge}} = 1$). For this scenario, a hexapedal arrangement is projected with three actuators active at any one-time (or $C + C_p \approx 4nF$), a step frequency (with payload) of approximately 20 Hz, a thin-film Li-ion battery with $\rho \approx 80$ W/kg (estimated from battery description in [17]), and a efficiency of a boost converter of $\eta \approx 15\%$ (projected from trends in [18], [19]). Under these circumstances, reducing the number of charging events results in a reduction in necessary battery mass of 5.2 mg, to remaining battery mass of 2.6 mg, and need for three 1 mg inductors. In addition, it is clear that significant challenges are placed on microrobotics due to low effective battery power densities when packaging is accounted for at small scales and very inefficient voltage conversion for low current loads (<1 μA average current for this system); this remains a major area of ongoing research.

The leg configuration used above corresponds to a previously proposed robot design with 4-mm-long legs and approximately 500 μm step lengths, and approximately an 8 mg payload after accounting for an approximately 1 mg mass of the robot chassis [16]. Thus, charge recovery can be envisioned as having a significant potential effect on meeting microrobot power requirements at very small scales using existing power supply and inductor technology. Other approaches, naturally, are possible, including omission of the charge recovery circuit and inductors and robot operation at lower stepping frequencies or voltages. Weight bearing capacity could potentially be increased by reducing leg length (and step distance) or step frequency. Either of the above options trades reduced power system mass for reduced robot speed. It should be emphasized, though, that realizing a real robot of of this type depends on significant further ongoing efforts to integrate multiple actuators and assemble them with the power circuitry, and thus the analysis above should be treated as merely illustrative of the impact that a charge recovery system might theoretically have.

VII. Conclusion

The incompatibility between capacitive loads (such as piezoelectric actuators) and traditional analog amplifiers is the motivation for considering a nonconventional motion control strategy. The simplest alternative is an optimal ON–OFF controller. Our next step was to incorporate a charge recovery circuit, which saves a portion of energy drained from the actuators when voltage is discharged. Compared to the two possible input values of a pure ON–OFF controller, a partial charge recovery controller has four or more different input levels which makes the optimization problem more complex. However, the additional input levels make the controller more flexible and allow it to span more points in the state space over a given time period, and the incorporated charge recovery can decrease actuator power consumption. An integer programming-based optimization method was used to minimize the energy consumed by an MEMS piezoelectric actuator-charge recovery system. The optimization incorporated both the dynamics of the actuator as well as circuitry constraints. The benefit of this optimization is shown as the savings in the combined weight of a battery and the related circuitry, as well as improved accuracy in motion.

To minimize the weight on board a microrobot for a given motion, the partial charge recovery strategy is also advantageous for reducing the necessary inductor size needed to recover some energy from the actuator. Although this only saves a fraction of the energy drained (compared to a complete charge recovery), it enables the flexible controller and reduces the necessary size and weight of inductors. A sample scenario based on projected capabilities of prototype robotic leg joints in a microscale robot and performance of the charge recovery controller is provided to illustrate potential benefits of the proposed controller. Since the actuator is designed for an autonomous microrobot which will walk in a quasistatic manner, in practice the final angle achieved by the controller would be intended to be the optimum angle for a particular gait. In practice, under certain circumstances the net effect of the charge recovery controller implementation can be to reduce overall mass of a microrobotic power system significantly, while enabling smoother desired motions from piezoelectric actuators. It should additionally be noted that the current work does not address inefficiencies of the power supply (either many batteries in series or a voltage converter connected to a capacitor), which have a large effect on overall system efficiency. In either case, however, charge recovery should be able to dramatically reduce the amount of power that must be delivered at high voltages.

The control strategy provided here is limited, however, in that it is only directly applicable to control of transient motions of actuators that appear as capacitive loads. Primary examples of these include the piezoelectric actuators discussed in this paper, as well as capacitive or electrostatic actuators also common in MEMS technology. Model-predictive control approaches may

be used with a receding horizon, but with the need to continually resolve the optimization problem, where open-loop implementation can use precomputed switching sequences. For example, the integration of sensors into the microrobotic leg joints presented here has not yet been successful, so only an open-loop controller is implemented. In this situation, the disadvantage is that the performance of the system depends on the accuracy of the identified model and the robustness of the controller is limited. In addition, capacitance and leakage properties of thin-film PZT are often highly variable, often requiring characterization on a wafer-by-wafer basis; this can sometimes inhibit implementation of more complex, but potentially more efficient, switching sequences (such as those computed for multiple charge-discharge cycles or multiple repeated motions), as they require progressively greater accuracy in leakage and capacitance measurements. These more advanced strategies are potentially better suited, then, to direct electrostatic capacitive actuation or use with bulk-ceramic piezoelectric actuators. Finally, the discrete input voltages of switching controllers can excite the higher order dynamics of the system. The effect of these dynamics on the final state can be captured by identifying a higher order model for the system, but the oscillations due to the higher dynamics would not be completely eliminated using this approach. Nonetheless, results of controller testing on prototype robot leg joints indicate benefits in building a controller which consumes minimum energy and is capable of being deployed on an autonomous microrobot. In addition, from the experimental results it is seen that most characteristics of the microrobotic leg can be captured using careful system identification and acceptable performance can be obtained in laboratory conditions, although the effects of operation in changing environments remains a topic for further study.

ACKNOWLEDGMENT

The authors thank the Army Research Laboratory in Adelphi, MD, for sample thin-film piezoelectric actuators.

REFERENCES

[1] M. Mohhebi, M. Terry, K. Böhringer, G. Kovacs, and J. Suh, "Omnidirectional walking microrobot realized by thermal microactuator arrays," in *Proc. 2001 ASME Int. Mech. Eng. Congr.*, New York, pp. 1–7.

[2] A. Bonvilain and N. Chaillet, "Microfabricated thermally actuated microrobots," in *Proc. 2003 IEEE Int. Conf. Robot. Autom.*, Taipei, Taiwan, pp. 2960–2965.

[3] T. M. Ebefors, U. Johan, E. Kälvesten, and G. Stemme, "A walking silicon micro-robot," in *Proc. 10th Int. Conf. Solid-State Sens. Actuat.*, Sendai, Japan, 1999, pp. 1202–1205.

[4] S. Hollar, A. Flynn, C. Bellow, and K. Pister, "Solar powered 10 mg silicon robot," in *Proc. 16th IEEE Annu. Int. Conf. Micro Electro Mech. Syst. (MEMS) 2003*, Kyoto, Japan, pp. 706–711.

[5] R. Linderman and V. Bright, "Nanometer precision positioning robots utilizing optimized scratch drive actuators," *Sens. Actuat. A, Phys.*, vol. A91, no. 3, pp. 292–300, Jul. 2001.

[6] B. Donald, G. Levy, C. McGray, I. Papotry, and D. Rus, "An untethered electrostatic, globally controllable mems micro-robot," *J. Microelectromech. Syst.*, vol. 15, no. 1, pp. 1–15, Feb. 2006.

[7] E. Steltz, M. Seeman, S. Avadhanula, and R. S. Fearing, "Power electronics design choice for piezoelectric microrobots," in *Proc. IEEE/RSJ Int. Conf. Intell. Robots Syst.*, 2006, pp. 1322–1328.

[8] M. Sitti, "Piezoelectrically actuated four-bar mechanism with two flexible links for micromechanical insect thorax," *IEEE/ASME Trans. Mechatronics*, vol. 8, no. 1, pp. 26–36, Mar. 2003.

[9] K. Oldham, J. Pulskamp, R. Polcawich, and M. Dubey, "Thin-film pzt actuators with extended stroke," *J. Microelectromech. Syst.*, vol. 17, no. 4, pp. 890–899, Aug. 2008.

[10] E. Sarajlic, E. Berenschot, N. Tas, H. Fujita, G. Krijnen, and M. Elwenspoek, "Fabrication and characterization of an electrostatic contraction beams micromotor," in *Proc. 19th IEEE Int. Conf. Micro Electro Mech. Syst. (MEMS)*, Istanbul, Turkey, Jan. 2006, pp. 814–817.

[11] J. Main, D. Newton, L. Massengill, and E. Garcia, "Efficient power amplifiers for piezoelectric applications," *Smart Mater. Struct.*, vol. 5, no. 3, pp. 766–775, Aug. 1996.

[12] B. Edamana, B. Hahn, J. S. Pulskamp, R. G. Polcawich, and K. Oldham, "Modeling and optimal low-power on-off control of thin-film piezoelectric rotational actuators," *IEEE/ASME Trans. Mechatronics*, vol. 16, no. 5, pp. 884–896, Oct. 2011.

[13] D. Campolo, M. Sitti, and R. S. Fearing, "Efficient charge recovery method for driving piezoelectric actuators with quasi-square waves," *IEEE Trans. Ultrason., Ferroelectr., Freq. Control*, vol. 50, no. 3, pp. 237–244, Mar. 2003.

[14] A. Bemporad and N. Girogetti, "A sat-based hybrid solver for optimal control of hybrid systems," *Lecture Notes Comput. Sci.*, vol. 2993, pp. 126–141, 2004.

[15] K. Oldham, J. Pulskamp, R. Polcawich, P. Ranade, and M. Dubey, "Thin-film piezoelectric actuators for bio-inspired micro-robotic applications," *Integrated Ferroelectr.*, vol. 95, no. 1, pp. 54–65, Dec. 2007.

[16] K. Oldham, C.-H. Rhee, J.-H. Ryou, R. Polcawich, and J. Pulskamp, "Lateral thin-film piezoelectric actuators for bio-inspired micro-robotic locomotion," in *Proc. 3rd Int. Conf. Micro Nano Syst.*, San Diego, CA, Aug. 2009, pp. 759–768.

[17] W. West, J. Whitacre, E. Brandon, and B. Ratnakuma, "Lithium microbattery development at the jet propulsion laboratory," *IEEE AESS Syst. Mag.*, pp. 31–34, 2001.

[18] L. Technologies, "Micropower dc/dc converter with programmable peak current limit," *cds.linear.com*, pp. 1–16, 2002.

[19] M. Karpelson, G.-Y. Wei, and R. Wood, "Milligram-scale high-voltage power electronics for piezoelectric microrobots," in *Proc. Int. Conf. Robot. Autom.*, Kobe, Japan, May 2009, pp. 2217–2224.

Biju Edamana received the B.Tech. degree in mechanical engineering from the National Institute of Technology, Calicut, India, in 2004, and the M.S. degree in mechanical engineering from the University of Michigan, Ann Arbor, in 2008, where he is currently working toward the Ph.D. degree.

His current research interests include developing low-energy control strategies for microrobotics, under development in the Vibrations and Acoustics Laboratory, University of Michigan.

Kenn R. Oldham (M'09) received the B.S. degree in mechanical engineering from Carnegie Mellon University, Pittsburgh, PA, in 2000, and the Ph.D. degree in mechanical engineering from the University of California, Berkeley, in 2006.

He is currently an Assistant Professor in the Department of Mechanical Engineering, University of Michigan, Ann Arbor. His research interests include microactuator design and applications, optimal design and control, design for controllability, and efficient sensing and power strategies for MEMS devices.

Prof. Oldham is a member of the American Society of Mechanical Engineers.